

See discussions, stats, and author profiles for this publication at: <https://www.researchgate.net/publication/235217271>

Influence of Zeolite Surface in the Sorption of Methane from Molecular Dynamics

ARTICLE *in* THE JOURNAL OF PHYSICAL CHEMISTRY C · JUNE 2011

Impact Factor: 4.77 · DOI: 10.1021/jp202043t

CITATIONS

13

READS

24

2 AUTHORS:



Aldo Fabrizzio Combariza Montañez

Universidad de Sucre

19 PUBLICATIONS 96 CITATIONS

[SEE PROFILE](#)



German Sastre

Research Scientist

118 PUBLICATIONS 2,366 CITATIONS

[SEE PROFILE](#)

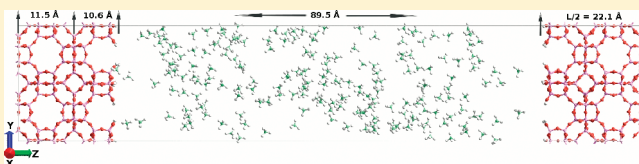
Influence of Zeolite Surface in the Sorption of Methane from Molecular Dynamics

Aldo F. Combariza and German Sastre*

Instituto de Tecnología Química, Universidad Politécnica de Valencia, Consejo Superior de Investigaciones Científicas, Av de Los Naranjos S/N, 46022 Valencia, Spain

 Supporting Information

ABSTRACT: We report results of molecular dynamics simulations on the transient and equilibrium surface adsorption of methane in a model Si-LTA zeolite structure with explicit silanol terminal groups. Using probability occupancy maps, 2D occupational densities, and free energy profiles, we extract a microscopic picture of the adsorption process, showing surface preferential zones of interaction around the partially exposed oxygen atoms of the surface silanol groups due to attractive silanol–guest attractions. The global effect of the loading on the uptake process is observed as a decrease in the free energy barrier as the loading increases and an increase in the surface permeability, calculated either from the initial uptake transient process or from equilibrated trajectories. The order of magnitude of the obtained surface permeability suggests a barrier that becomes relevant to the overall mass transfer for crystal sizes in the range of a few unit cells. Our results support experimental evidence that ascribe surface resistances to severe crystal structure deviations, causing an almost complete blockage of the surface available entering windows.



INTRODUCTION

Microporous crystalline materials such as zeolites are extensively used in a wide set of industrial applications because of special characteristics like large free volume, low density, void spaces in form of cages and channels, thermal stability, and acid/base properties.¹ Catalysis,^{2,3} adsorption,⁴ ion exchange, electronics,⁵ molecular sieving,^{6,7} and many other interesting applications^{1,8,9} are known fields of application for these materials, with recent efforts being directed toward the synthesis of zeolites with extra large pores.¹⁰ In the past years, an appreciable effort has been devoted to the study of the underpinning phenomenology of diffusion and adsorption processes of species confined in nanoporous materials. Special mention deserves the work of Jörg Kärger, who has brought the attention of the research community back to the fundamental diffusional processes.^{11–13} With the help of enhanced experimental techniques, such as pulse field gradient NMR (PFG-NMR) and high-resolution transmission electron microscopy (HR-TEM),¹⁴ there is now an open window to study the molecular motion on length scales small enough to appreciate the true intracrystalline displacements of the guest phase as well as to analyze transport resistances due to defects and surface effects.^{14–18} Nevertheless, the ongoing research efforts have been centered in the transport of the guest phase within the host materials, whereas the influence of surface barriers and structural defects in molecular sorption and release processes has just recently started to receive appropriate attention.^{16,18–31}

The modeling of zeolite surfaces has been closely associated with advances in the experimental characterization of solids. Experimental studies on this subject, applying techniques such as HR-TEM³² to elucidate the external surface structure

of silicalite-1 zeolite or the use of atomic-force microscopy (AFM) to investigate the details of the external surface of mordenite (MOR), HEU, and LTA zeolites,^{33,34} have provided the necessary information to model the structural intricacies of the surfaces in these materials. Several force fields accounting for silanol groups at the external surface of zeolites have been developed and used recently in either lattice calculations and molecular dynamics simulations (MD).^{21,23,29,35–37} In this work, we used an MD approach to study the influence of the surface on the transient and equilibrium sorption process of methane in a model Si-LTA zeolite with explicit surface silanol groups. Zeolite Si-LTA (ITQ-29) was chosen as a model because of the extensive amount of experimental and computational data collected over the years and given its importance in the industrial field. Slater et al. have recently published a study on Si-LTA in which the stability of the surface structure is characterized via lattice calculations.²¹ Their computational study complemented experimental HRTEM measurements³⁴ that were not entirely conclusive about the surface structure of this zeolite. We used the conclusions of their work about the possible most stable surface termination on Si-LTA to create a slab model with specific silanol surface groups to study the process of methane being adsorbed through its surface. The transient flux of methane is measured by following the time-dependent entrance of guest molecules across the surface of the framework until a condition of zero net flux is reached. According to Fick's second law, this flux can be related to the net change of concentration through a parameter

Received: March 3, 2011

Revised: June 8, 2011

Published: June 23, 2011

encompassing all resistances to the mass-transfer due to the surface topology. Our results suggest an uptake process well described by exponential functions, with characteristic times dependent on the loading level. As we will see below, a microscopic picture capturing the details of the dynamical sorption process was drawn from the molecular dynamics calculations described and discussed in the present communication.

METHODS

Zeolite Surface Model. Zeolite ITQ-29 (all silica LTA framework type) has a 3D network of spherical cavities (α -cages) of ~ 11.4 Å in length, interconnected by six small eight-ring windows with effective diameter of 4.1 Å.³⁸ Likewise, all silica LTA can be described as a structure made of sodalite cages (β -cages) connected through the square faces with each other, forming double four-ring (D4R) units. Figure 1 shows the single four-ring (S4R), double four-ring edge (D4R-e), and double four-ring final (D4R-f) configurations for Si-LTA {100} surface, according to the terminology adopted by Slater et al.²⁹ Their calculations show that the S4R configuration was more stable than the D4R configuration, in opposition to experimental results,^{33,34} although the discrepancy could be ascribed to kinetic stability issues or to the presence of stabilizing ions in the

synthesis solution. On the basis of the stability calculations of Slater et al., we decided to model the D4R-e terminal silanol configurations because this configuration also agrees with atomic force microscopy (AFM) determinations of LTA surfaces.³³ Simulation cells are generated by appropriate scaling of experimental unit cells, followed by cutting and replacing the surface pure SiO units by SiOH groups. Table 1 shows the details of ITQ-29 cell parameters and the number of atoms in the simulation cell.

Details of Computational Method. We used an MD approach to simulate the sorption process of methane in contact with a model all-silica LTA framework with explicit terminal silanol groups at the surface (see details of the simulation cell in Figure 2) using the general purpose DL_POLY_2.20 code.³⁹ The space between the zeolite layers is initially filled with methane molecules, and the system is allowed to relax until equilibrium is reached. We monitored the flux of methane inside the framework by counting the number of molecules that pass through the surface until the number of molecules crossing within the zeolite layer is equilibrated with the number of molecules reaching the interlayer region, that is, until no net flux of methane exists.

The potential energy surface of the system takes into account three main terms (eq 1): the zeolite potential energy, V^{Zeo} , the methane potential energy, V^{M} , and the intermolecular potential

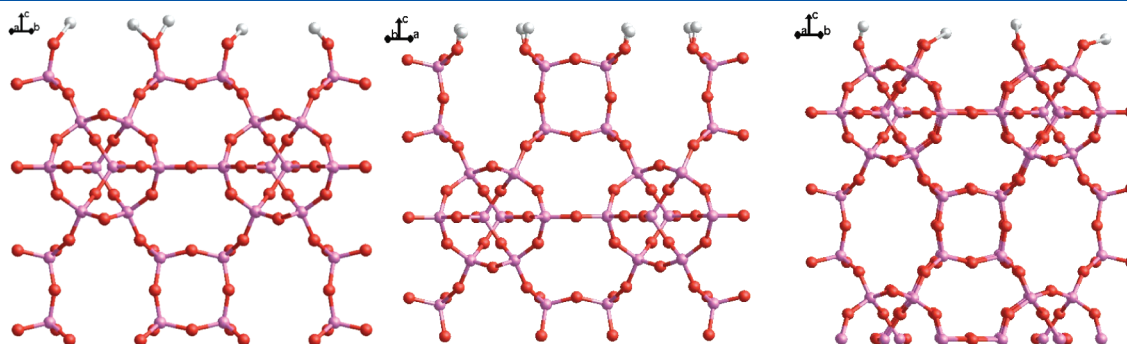


Figure 1. Hydroxylated pure Si-LTA zeolite {100} surfaces: left S4R, center D4R-edge, and right D4R-f termination. Red, violet, and white dots correspond to silicon, oxygen, and hydrogen atoms, respectively.

Table 1. Pure Silica LTA Zeolite: Lattice Parameters and Simulation Cell Size

zeolite	a [Å]	b [Å]	c [Å]	$\alpha = \beta = \gamma$ [deg]	pure $\text{SiO}_{4/2}$ sim. cell.	sim. cell. + surface
(ITQ-29) LTA ³⁸	11.92	11.92	11.92	90.0	$2 \times 2 \times 4 - 1152$ atoms	$2 \times 2 \times 4 - 1008$ atoms

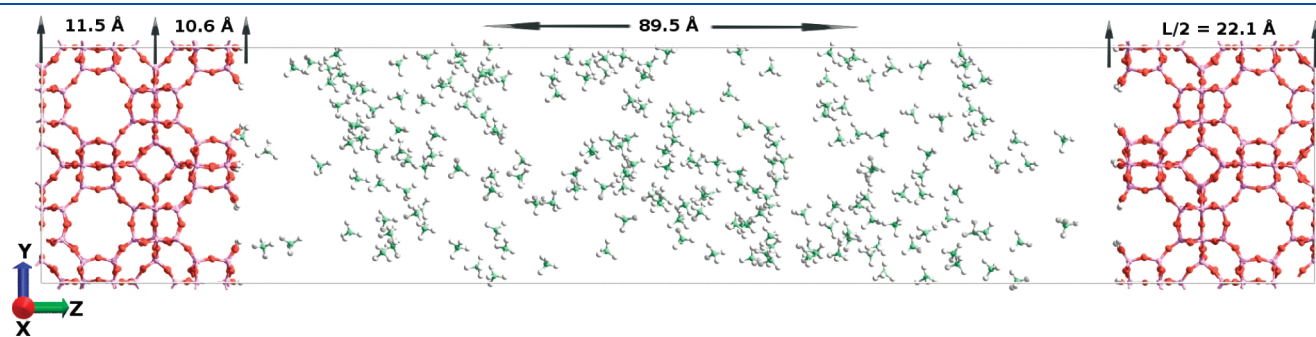


Figure 2. Snapshot of the simulation cell with an initial content of 180 methane molecules in the interlayer space. Periodic boundary conditions are enforced in the XY and Z axis of the simulation cell. The replicated unit cell represents a zeolite layer infinitely extended along the XY plane, two unit cells wide at each edge of the Z axis, forming a membrane separated by an interlayer space 89.5 Å in length.

energy contribution, $V^{\text{Zeo}-\text{M}/\text{M}-\text{M}}$

$$V^{\text{total}} = V^{\text{Zeo}} + V^{\text{M}} + V^{\text{Zeo} - \text{M}/\text{M} - \text{M}} \quad (1)$$

The intramolecular potential for methane comprises two-body (bond) interactions plus electrostatic Coulomb terms. Parameters for this potential are given in the original reference by Oie et al.⁴⁰ Lennard-Jones (LJ) potentials are used to describe the intermolecular host–guest and guest–guest interactions modeled via the 12–6 LJ functional form.

Initially, we have modeled the system including framework flexibility using the Sanders et al.⁴¹ FF to model the bulk of the framework, extended with the Baram–Parker⁴² FF to represent the surface silanol groups in a similar fashion to the recent work of Gren et al.²¹ These FF values are based on the core–shell model, which requires to set an integration time-step of the order of 0.02 fs, a value small enough to avoid any energy exchange with the guest molecules and to model properly the O–H vibrational frequencies. However, this small integration time step has the inconvenience of extending the simulation times beyond computational efficient limits. Therefore, full framework flexibility was initially included in our MD calculations to test the possible impact in the short- and long-range dynamics of the system. As suggested in previous computational studies for the specific system Si-LTA/methane,^{7,43} the effect of framework flexibility on guest long-range mobility is negligible because the size of the 8MR is large enough to not significantly hinder the intercage motion of the guest molecules. Initial tests, performed to evaluate this idea, suggested that framework flexibility does not have a major influence on methane dynamics, as calculated occupancy profiles for flexible (Supporting Information), and fixed frameworks do not differ significantly. In view of this fact, we decided to follow a rigid framework approach, which allows us to extend the time length of the simulations within computational efficient limits.

The velocity-Verlet algorithm is used throughout to integrate the Newton's equations of motion with a time step of 1 fs. The number of molecules in the interlayer space is set from 20 to 200 molecules, with increments of 20 molecules. We sample microstates in the canonical (NVT) ensemble, setting the target temperature to 300 K by means of the Berendsen thermostat with a decaying time constant of 4 ps.⁴⁴ This thermostat is known to work efficiently in systems with large number of atoms by weakly coupling the system with an external heat bath. To initiate the transient surface adsorption process, we placed a given load of methane molecules in the vacuum space between the layers of the Si-LTA and allow the system to equilibrate for at least 4 ns. The methane placed in the interlayer section of the system was subject to a pre-equilibration MD calculation to guarantee the nonexistence of strange dynamical responses, which could emerge from a nonequilibrated system. Analysis of the trajectories is carried out from the history files generated to obtain 3D probability density maps and histogram sampling to obtain the occupancy probability density (OPD) along the specified adsorption coordinate and free energy profiles.^{45,46}

Surface Transport Resistance. We model the transient sorption process by following the time-dependent variation of the number of guest molecules ($N(t)$) reaching the interior of the framework through the surface (A). The process will reach an equilibrium state once the number of molecules reaching the interior of the zeolite is balanced by the number of molecules leaving, thus having a zero net flux. The molecular exchange process between the gas phase and the host can be described by

Fick's second law (eq 2)

$$\frac{\partial c(z, t)}{\partial t} = \frac{\partial}{\partial z} D \frac{\partial c(z)}{\partial z} \quad (2)$$

with D being the Fick's diffusion coefficient of the guest, which will contain all of the resistances to the mass transfer process. At the interface ($z = 22.1 \text{ \AA}$, see Figure 2), we can define the flux of molecules passing through the surface, $j(t)$, as the limiting case of the Fick's second law, where z is the coordinate that represents the concentration gradient

$$j(t) = \alpha_s(C(t)_{\text{eq}} - C(t)) = \frac{1}{2A} \frac{dN(t)}{dt} \quad (3)$$

where $C(t) = (N(t))/(AL)$ is defined as the concentration of molecules actually in the boundary region (surface), $C(t)_{\text{eq}}$ is the concentration that is at equilibrium with the bulk gas phase ($C(t)_{\text{eq}}$), and α_s (see eq 4) is the surface permeability, which will be the parameter enclosing the information relative to the surface resistance to the mass transfer process. Factor 2 in eq 3 arises from the fact that the flux coming into the zeolite passes through both sides of the zeolite layer, which makes the exposed area two times the cross section area of the unit cell.

$$\alpha_s = \frac{L}{2(N(t)_{\text{eq}} - N(t))} \frac{dN(t)}{dt} \quad (4)$$

From the MD trajectories, we can readily obtain the time-dependent number of molecules reaching the interior of the zeolite, $N(t)$, the variation of the number of molecules in the gas phase, and therefore the number of molecules at equilibrium with the gas phase, $N(t)_{\text{eq}}$.

RESULTS AND DISCUSSION

We have initially checked the consistency of our potential model by comparing the amount of methane adsorbed with adsorption isotherms available in the literature for the system all-silica LTA zeolite and methane.^{47,48} We found that the amount of methane adsorbed in our zeolite model, corresponding to the average number of molecules in the interior of the zeolite model at equilibrium, agrees with existent data for the adsorption isotherms in the system Si-LTA-methane. Under the initial condition of 200 molecules, we calculate a maximum amount adsorbed of approximately seven molecules per α -cage. The saturation value for methane in Si-LTA zeolite, extracted from published isotherms, is calculated to be ~ 16 molecules per α -cage, and thus our calculations are located in a low-to-medium pressure region in the adsorption isotherms. The amount of methane adsorbed in our system also suggests that we are in a situation where the intracrystalline guest diffusional constant follows an increasing pattern with loading. This guarantees that loading-dependent diffusional effects will not exert a strong influence in the modeled adsorption process.

Occupancy Probability Density and Free Energy Profiles. Figure 3 shows plots of OPD of methane molecules along the adsorption coordinate (Z axis in our model system), obtained from equilibrated trajectories under different conditions. Additionally, Figure 3 shows the calculated mean free energy profiles, corresponding to the probability density of the guest molecules at equilibrium. Three regions are readily identified from the plot: the interlayer space corresponding to $z (\text{\AA}) \geq 22.1 \text{ \AA}$, an intermediate region corresponding to the surface-exposed

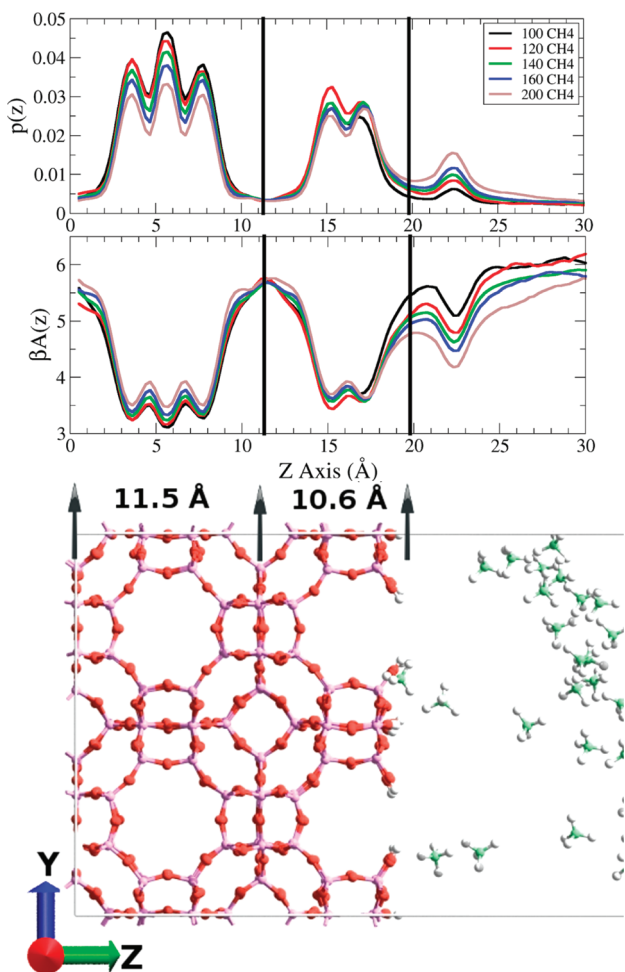


Figure 3. Occupancy probability density $P(z)$ (top) and mean free energy profiles (bottom), as experienced by guest molecules obtained from histogram sampling of equilibrated MD trajectories ($500 \text{ ps} < t > 10 \text{ ns}$) at different loadings of methane. Thick vertical lines correspond to the location of the internal eight-rings perpendicular to the adsorption coordinate (left most) and to silanol groups located at the surface of the structure (right).

partially cleaved α -cages between $11.5 \leq z (\text{\AA}) < 22.1$, and the interior zone located in the range $0 < z (\text{\AA}) \leq 11.5$ comprising full α -cages limited along the z axis by eight-member ring windows.

The region at the external surface of the zeolite, $z \geq 22.1 \text{ \AA}$ in Figure 3, shows the existence of a preferential siting zone for the guest molecules, clearly captured by the concentration-dependent peak just beyond the terminal silanol groups. This suggests that the external surface offers a preferential region for surface adsorption, which could be rationalized as a consequence of attractive van der Waals interactions arising between the external hydrogen groups of the methane molecules and the surface partially exposed oxygen atoms of the silanol groups. This behavior is confirmed by looking at the 2D plot showing the outermost layer of silanol groups and the OPD regions located just between the OH groups shown in dark (red online) in the left plot of Figure 4. Comparison of the OPD at the internal regions of the system with the size of the surface OPD shows that the number of events occurring at the favorable external surface interaction zone is only a limited fraction of the total number of surface-passing events through the external interface; this makes statistical sense because the open accessible area of the surface is larger than the structurally limited D4R endings of the zeolite. A second feature of the surface region is the concentration dependence, which is clearly visible at the OPD in Figure 3, with probability densities growing as a function of increasing number of methane molecules at the interlayer region.

The region between the external surface of the zeolite and the first eight-member window along the z axis, located between the thick black lines in Figure 3, is qualitatively different from that of the external surface and the actual intracage environment. There are only two peaks in the OPD plot of Figure 3, reflecting the fact that the partially cleaved α -cages actually limit the number of preferential adsorption sites. A salient feature in this zone is given by the low density population in the center of the cleaved-cage, right peak in the region between $11.5 \leq z (\text{\AA}) < 22.1$, which translates as a limitation in the number of crossing events along the X and Y axis of the simulation cell. The diffusion of the guest phase in the XY plane is heavily influenced by the environment of

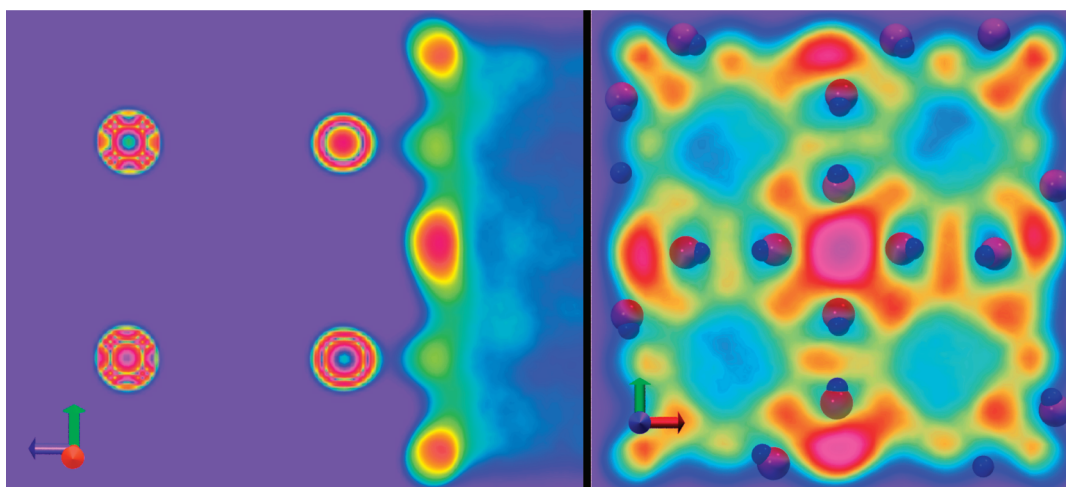


Figure 4. Methane equilibrium occupancy volume slice along the Z axis, cutting plane ZY at the middle of the simulation cell (left). Methane occupancy volume slice at the cutting plane XY on top of the silanol groups (right) from a 3D volume map of a MD trajectory at initial loading of 160 methane molecules. High occupancy density zones are shown in red and vanishing occupied zones in blue/violet. The positions of the OH groups at the surface are shown as red (O) and blue (H) spheres in the plot at right.

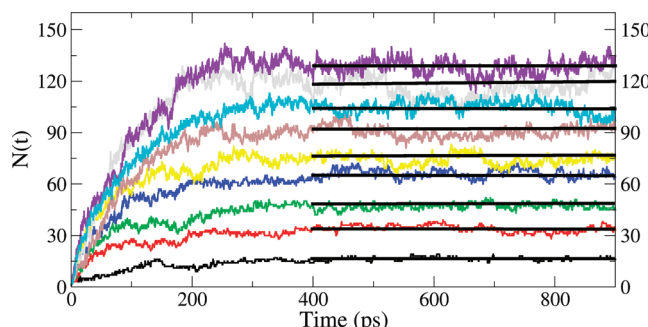


Figure 5. Time-dependent variation of the number of molecules reaching the interior of the zeolite ($N(t)$). Curves correspond to initial loadings, that is, molecules initially placed within the interlayer space, varying from 20 to 200 molecules from bottom to top. Equilibrium average number of molecules is represented by linear fits in the regions beyond 400 ps, where stabilization of the flux has been reached.

the cleaved α -cages, driving the guest toward the entropic barrier given by the first eight-member ring of the internal cavities, limiting the displacements in the XY plane. The free energy distinctive regions shown in Figure 3, separated by the XY planes between $z = 0$ and 22.1 Å, indicate that under equilibrium conditions the framework confinement effect changes as a function of the z coordinate, weaker at the surface and at the partially cleaved initial structure and becoming stronger at the interior of the zeolite. This behavior is also dependent on the initial number of guest molecules, with larger changes arising at the surface region located at z (Å) \geq 22.1 Å. An insightful analysis was published recently by Zimmerman et al.²⁰ for adsorbed gases in an AFI-type zeolite using a computational approach based on the MC method and the dynamically corrected transition state theory. They carefully analyze the equilibrium free energy profiles experienced by methane and ethane at the external crystal surface at different concentrations, finding a strong dependence on this parameter, which causes the formation of a liquid layer on top of the surface. By comparison with our results, the effect of the structure on the sorption process is clearly appreciated.

The microscopic picture extracted from the free energy and occupancy profiles obtained suggest a surface adsorption process at equilibrium initially limited by the available area of the external surface, where a fraction of the incoming molecules stick to the favorable zones with exposed surface oxygen atoms and then creep toward the interior zones and a larger fraction of guest molecules passing through the nonentropic-limited surface area. The initial adsorption is then followed by a mass transfer process driven along the Z coordinate, limited in the XY plane by the partially cleaved α -cages at the surface and finally the process becomes comparable to the purely intracrystalline diffusional process limited by the internal eight-ring entropic barriers. The global effect of the initial concentration on the uptake process is observed at the external surface as a decrease in the free energy as the concentration increases. This effect is driven by entropic contributions due to increasingly limited mobility caused by growing number of interacting molecules in this region.

Surface Permeability. The short- and long-range uptake process is illustrated in Figure 5. The profiles correspond to initial conditions going from 20 to 200 molecules initially placed in the interlayer space. The transient uptake process is clearly seen from the depicted profiles, providing the information for the time variation of the number of molecules crossing the surface

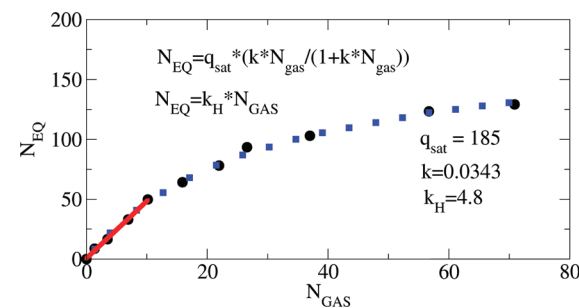


Figure 6. Isotherm representing the number of molecules within the pores of the zeolite, which are at equilibrium with a given concentration of methane molecules in the gas phase. The red line corresponds to region where a Henry isotherm could be applied and the discontinuous line represents the fit to a Langmuir isotherm. Text shows Langmuir isotherm fit and Henry isotherm applicable region as well as parameters.

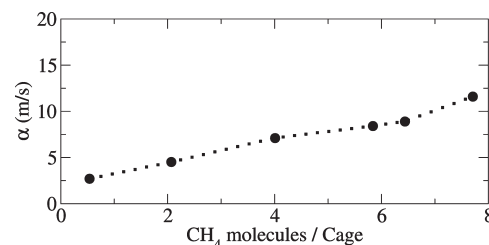


Figure 7. α_s values calculated from the MD data using the definition given by eq 4. The dotted line is drawn to indicate the increasing trend of α_s with concentration.

and actually reaching the interior of the framework. The profiles can be fit to single exponential functions with the general form $\Delta N(t) = N_0 - N_0 \exp(-t/\tau)$; the time constants (τ) are thus extracted from the fitting procedure. Equilibrium conditions are represented by horizontal lines obtained through a linear regression of the curves for times beyond 400 ps. This limit corresponds to the situation of vanishing net flux of molecules through the surface. From the equilibrated simulations, we extracted the isotherm corresponding to the number of methane molecules adsorbed in equilibrium with the gas bulk phase; the data are depicted in Figure 6.

The α_s values calculated using the definition given by eq 4 and the data collected from the MD simulations fluctuate from 2.5 to 12 m/s, with an increasing pattern following the concentration of adsorbed methane. The α_s values are depicted in Figure 7. In a recent work by Thompho et al.,²³ NEMD calculations were performed in the system silicalite-1-methane by developing an FF that models the behavior of explicit silanol groups at the surface of the framework. Their model unit cell is similar in size to the model studied here, with obvious differences presented by the frameworks: 1D straight channel with 10-member ring-openings in the case of silicalite and the 3D network of cages separated by 8-member ring windows in the case of Si-LTA. In their analysis of the resistance of the surface to the mass transport, they find a time-dependent surface permeability, $\alpha_s(t)$, directly depending on the variation of the flux with time. Nevertheless, the values of α_s , obtained in their analysis for a system with surface silanol groups for constant concentration of the guest, are in the range 5–28 m/s. The values obtained in our work are comparable in magnitude, having in mind the topology

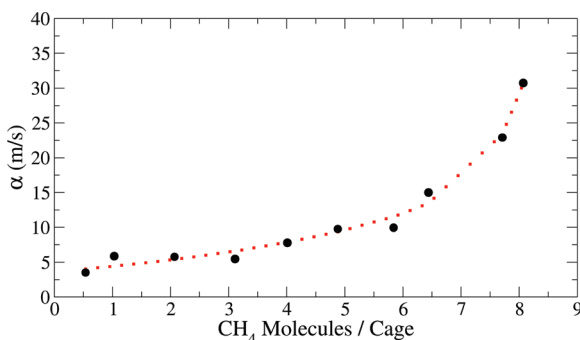


Figure 8. α_s^E values (●) calculated from MD data using the analytical expression (eq 5) of Schüring et al.⁴⁹ The dotted line is drawn to help the eye to follow the trend of α_s^E .

of silicalite-1, which will present a lower entropic barrier to the surface uptake and intracrystalline diffusivity of methane.

A second source of valuable data for the system Si-LTA/methane comes from the work of Schüring et al.⁴⁹ They have studied the surface mass-transfer process from an analytical point of view, developing a simplified model able to quantify the surface resistance under conditions of sorption equilibrium (α_s^E). Their analytical model corresponds to the tracer-exchange experiment, characterized by the zero net flux through the surface, according to the relation

$$\alpha_s^E = P_{\text{enter}} \frac{\nu}{K} \quad (5)$$

with P_{enter} defined as the ratio between the number of molecules actually reaching the interior of the crystal and the total number of molecules hitting the surface within a certain period of time,⁵⁰ $\nu = 158$ m/s being the mean terminal velocity of a molecule of mass, m , traveling at temperature T , and K represents the ratio of molecular densities in the boundary layer of the zeolite and the gas phase.

The α_s^E value from the analytical expression of Schüring et al. for sorption equilibrium of three methane molecules per zeolite cage is equal to 1.5 m/s at 300 K. In their work, the P_{enter} parameter under the previously specified conditions takes a value of 0.05. P_{enter} calculated from our MD data under similar conditions produces a value of 0.17, more than three times larger than that of the analytical model. The parameter K is comparable in both cases, with value of 5.4 and 4.9, corresponding to Schüring's and our work, respectively. With the parameters extracted from our MD calculations, the calculated value of α_s according to eq 5 would be 5.47 m/s. This larger value could be rationalized taking into account that there is a surface region in our model, which favors the sticking and subsequent creeping of guest molecules inside the framework, thus increasing the P_{enter} value. This favorable zone does not exist in the model simulated by Schüring et al., and as a consequence, their α_s values indicate a more restricted surface mass-transfer process. The equilibrium α_s^E obtained from eq 5 is depicted in Figure 8 for the set of conditions used in our MD simulations. The depicted α_s^E values follow a growing tendency with loading, similar to that reported by Schüring.

On the basis of the calculated values of α_s , we have determined the conditions for which the surface barrier will become relevant in comparison with purely intracrystalline diffusional resistances. The effective resistance as defined by Kärger and Ruthven¹³ is

given by

$$\tau = \tau_{\text{diff}} + \tau_{\text{barr}} = \frac{R^2}{15D} + \frac{R}{3\alpha_s} \quad (6)$$

which comes from the first statistical moments of the uptake curves, with R being the radius of a sphere representing the shape of the adsorbent. The limiting case of diffusion control and surface barrier control will be represented by $\tau_{\text{diff}} = (R^2)/(15D)$ and $\tau_{\text{barr}} = (R)/(3\alpha_s)$, respectively. Surface resistances will thus become significant if $(\tau_{\text{diff}})/(\tau_{\text{barr}}) = (5D)/(R\alpha_s) > 1$ or when the particle diameter R is smaller than $(5D)/(\alpha_s)$. Values for self-diffusion coefficients of methane in pure silica LTA zeolite calculated previously⁶ are close to 6×10^{-9} m²/s, and with the α_s values obtained here, it is found that surface effects will become relevant for particles with radii in the order of 10 Å, which is just about the dimensions of a unit cell. This result is in perfect agreement with the experimental evidence on the surface resistances in nanoporous materials recently published.^{15,16,25} In these works, it is shown that surface resistances on actual crystals must be connected with more severe structural imperfections in the material; actually, almost a total blocking of the surface access is needed to render a resistance large enough to be relevant for the overall kinetics.

CONCLUSIONS

In this work, we report results of MD simulations on the transient and equilibrium surface adsorption of methane in a model Si-LTA zeolite structure with explicit silanol terminal groups. Details of the microscopic surface uptake process were obtained by calculating the OPD and free energy profiles of methane from MD trajectories. The adsorption process along the Z coordinate in our model system shows surface preferential zones of interaction with the guest phase due to attractive van der Waals interactions. From 2D occupancy maps, we locate the preferential interaction zones between the partially exposed oxygen atoms belonging to the surface silanol groups. The external surface adsorption process is followed by a mass transfer driven along the Z coordinate and limited in the XY plane by the partially cleaved α-cages at the surface. The surface permeabilities calculated using either MD data or the analytical equation of Schüring et al. increase as a function of the loading, in agreement with experimental measurements. On the basis of the α_s values obtained in this work and on previously measured diffusion coefficients for the same system, we show that only for crystals scarcely larger than the unit cell dimensions may the determined surface resistances become relevant for the overall mass transfer. This result agrees with experimental evidence of surface resistances in nanoporous materials⁵¹ and subsequent modeling and analytical treatment,⁵² where it is shown that the surface resistances on “real” nanoporous crystals must be referred to much more severe deviations in the crystal structure, most likely a complete blockage with only a few open “windows” in the surface.

Force field modeling at the boundary between the genuine crystalline phase and the surrounding atmosphere in a regular way does not lead to surface barriers, which are experimentally observed with “real” crystals consisting typically of thousands of thousands of thousands unit cells. This result may be supported by the following reasoning: If we imply that the resistance exerted by the “external” windows, that is, by the windows connecting the boundary layer of pores with the surrounding atmosphere, has any significant influence on the uptake or release, then its

influence must compete the influence of many thousands of jumps that the molecules have to perform on their migration path toward the interior. The jump probability through these external windows (provided all of them or, at least a notable fraction, are open) has to be, therefore, much less (e.g., 1/100) than the jump probability through the “internal” windows, corresponding to an extremely high activation energy. Such high activation energies, however, are generally not observed.

The surface resistances estimated in this study may be, however, of immediate relevance for host–guest systems, which consist of very thin layers of nanoporous material.⁵³ Second, such estimates are also of relevance by considering the overall mass transfer in mesoporous zeolites.^{54–56} Here mass transfer between the intracrystalline space and the surrounding is intended to be accelerated by mass transfer between the micropore space and the mesopores. Under such conditions, the finite rate of mass transfer at the (internal) boundary between the mesopores and the microporous space might become of some relevance and hence their estimate as provided by the results of the present work.

■ ASSOCIATED CONTENT

S Supporting Information. Force field parameters, compared OPD for flexible Vs fixed framework, details of the pressure calculation of the gas bulk phase, adsorption data and video that shows the uptake process. This material is available free of charge via the Internet at <http://pubs.acs.org>.

■ AUTHOR INFORMATION

Corresponding Author

*E-mail: gsastre@itq.upv.es.

■ ACKNOWLEDGMENT

Funding through Ministerio de Ciencia e Innovación (project MAT2007-64682) and computing time from Red Española de Supercomputación are gratefully acknowledged. A.F.C. acknowledges a research fellowship provided by the Instituto de Tecnología Química UPV-CSIC. We thank an anonymous reviewer for very insightful comments.

■ REFERENCES

- (1) Corma, A. *J. Catal.* **2003**, *216*, 298–312.
- (2) Climent, M. J.; Corma, A.; Iborra, S. *Chem. Rev.* **2011**, *111*, 1072–1133.
- (3) Corma, A.; Díaz, U.; García, T.; Sastre, G.; Velty, A. *J. Am. Chem. Soc.* **2010**, *132*, 15011–15021.
- (4) Song, L.; Sun, Z.; Duan, L.; Gui, J.; McDougall, G. S. *Microporous Mesoporous Mater.* **2007**, *104*, 115–128.
- (5) Li, Z.; Johnson, M. C.; Sun, M.; Ryan, E. T.; Earl, D. J.; Maichen, W.; Martin, J. I.; Li, S.; Lew, C. M.; Wang, J.; Deem, M. W.; Davis, M. E.; Yan, Y. *Angew. Chem., Int. Ed.* **2006**, *45*, 6329–6332.
- (6) Combariza, A. F.; Sastre, G.; Corma, A. *J. Phys. Chem. C* **2011**, *115*, 875–884.
- (7) Combariza, A. F.; Sastre, G.; Corma, A. *J. Phys. Chem. C* **2009**, *113*, 11246–11253.
- (8) Corma, A. *Nature* **2009**, *461*, 182–183.
- (9) Sastre, G.; Corma, A. *J. Mol. Catal.* **2009**, *305*, 3–7.
- (10) Sun, J.; Bonneau, C.; Cantin, A.; Corma, A.; Diaz-Cabanillas, M. J.; Moliner, M.; Zhang, D.; Li, M.; Zou, X. *Nature* **2009**, *458*, 1154–1157.
- (11) Chmelik, C.; Heinke, L.; Valiullin, R.; Kärger, J. *Chem. Ing. Tech.* **2010**, *82*, 779–804.
- (12) Chmelik, C.; Kärger, J. *J. Chem. Soc. Rev.* **2010**, *39*, 4864–4884.
- (13) Kärger, J.; Ruthven, D. M. *Diffusion in Zeolites and Other Microporous Solids*; John Wiley and Sons: New York, 1992.
- (14) Chmelik, C.; Heinke, L.; Valiullin, R.; Kärger, J. *Chem. Ing. Tech.* **2010**, *82*, 779–804.
- (15) Ruthven, D. M.; Heinke, L.; Kärger, J. *Microporous Mesoporous Mater.* **2010**, *132*, 94–102.
- (16) Zhang, L.; Chmelik, C.; van Laak, A. N. C.; Kärger, J.; de Jongh, P. E.; de Jong, K. P. *Chem. Commun.* **2009**, 6424–6426.
- (17) Fernandez, M.; Kärger, J.; Freude, D.; Pampel, A.; van Baten, J. M. v.; Krishna, R. *Microporous Mesoporous Mater.* **2007**, *105*, 124–131.
- (18) Krutyeva, M.; Yang, X.; Vasenkov, S.; Kärger, J. *J. Magn. Reson.* **2007**, *185*, 300–307.
- (19) Roque-Malherbe, R.; Polanco-Estrella, R.; Marquez-Linares, F. *J. Phys. Chem. C* **2010**, *114*, 17773–17787.
- (20) Zimmermann, N. E. R.; Smit, B.; Keil, F. J. *J. Phys. Chem. C* **2010**, *114*, 300–310.
- (21) Gren, W.; Parker, S. C.; Slater, B.; Lewis, D. W. *J. Phys. Chem. C* **2010**, *114*, 9739–9747.
- (22) Karwacki, L.; Kox, M. H. F.; Matthijs de Witner, D. A.; Drury, M. R.; Meeldijk, J. D.; Stavitski, E.; Schmidt, W.; Mertens, M.; Cubillas, P.; John, N.; Chan, A.; Kahn, N.; Bare, S. R.; Anderson, M.; Kornatowski, J.; Weckhuysen, B. M. *Nat. Mater.* **2009**, *8*, 959–965.
- (23) Thompho, S.; Chanajaree, R.; Remsungenen, T.; Hannongbua, S.; Bopp, P. A.; Fritzsche, S. *J. Phys. Chem. A* **2009**, *113*, 2004–2014.
- (24) Newsome, D. A.; Sholl, D. S. *Microporous Mesoporous Mater.* **2008**, *107*, 286–295.
- (25) Kortunov, P. V.; Heinke, L.; Arnold, M.; Nedellec, Y.; Jones, D. J.; Caro, J.; Kärger, J. *J. Am. Chem. Soc.* **2007**, *129*, 8041–8047.
- (26) Newsome, D. A.; Sholl, D. S. *J. Phys. Chem. B* **2005**, *109*, 7237–7244.
- (27) Ahunbay, M. G.; Elliott, J. R.; Talu, O. *Adsorption* **2005**, *11*, 313–318.
- (28) Ahunbay, M. G.; Elliott, J. R.; Talu, O. *J. Phys. Chem. B* **2004**, *108*, 7801–7808.
- (29) Slater, B.; Titiloye, J. O.; Higgins, F. M.; Parker, S. C. *Curr. Opin. Solid State Mater. Sci.* **2001**, *5*, 417–424.
- (30) Arya, G.; Chang, H.-C.; Maginn, E. J. *J. Chem. Phys.* **2001**, *115*, 8112–8124.
- (31) Arya, G.; Maginn, E. J.; Chang, H.-C. *J. Phys. Chem. B* **2001**, *105*, 2725–2735.
- (32) Díaz, I.; Kokkoli, E.; Terasaki, O.; Tsapatsis, M. *Chem. Mater.* **2004**, *16*, 5226–5232.
- (33) Ono, S. S.; Matsuoka, O.; Yamamoto, S. *Microporous Mesoporous Mater.* **2001**, *48*, 103–110.
- (34) Wakihara, T.; Sasaki, Y.; Kato, H.; Ikuhara, Y.; Okubo, T. *Phys. Chem. Chem. Phys.* **2005**, *7*, 3416–3418.
- (35) Abril, D. M.; Slater, B.; Blanco, C. *Microporous Mesoporous Mater.* **2009**, *123*, 268–273.
- (36) Pedone, A.; Malvasi, G.; Menziani, M. C.; Segre, U.; Musso, F.; Corno, M.; Civarelli, B.; Ugliengo, P. *Chem. Mater.* **2008**, *20*, 2522.
- (37) Slater, B.; Catlow, C. R. A.; Liu, Z.; Ohsuna, T.; Terasaki, O.; Cambor, M. A. *Angew. Chem., Int. Ed.* **2002**, *41*, 1235–1237.
- (38) Corma, A.; Rey, F.; Rius, J.; Sabater, M. J.; Valencia, S. *Nature* **2004**, *431*, 287–290.
- (39) Smith, W.; Yong, C. W.; Rodger, P. M. *Mol. Simul.* **2002**, *28*, 385–471.
- (40) Oie, T.; Maggiore, T. M.; Christopherssen, R.; Duchamp, D. J. *Int. J. Quantum Chem., Quantum Biol. Symp.* **1981**, *8*, 1.
- (41) Sanders, M. J.; Leslie, M.; Catlow, C. R. A. *J. Chem. Soc., Chem. Commun.* **1984**, 1271–1273.
- (42) Baram, P. S.; Parker, S. C. *Philos. Mag. B* **1996**, *73*, 49–58.
- (43) Krishna, R.; van Baten, J. M. *J. Phys. Chem. C* **2010**, *114*, 18017–18021.
- (44) Berendsen, H. J. C.; Postma, J. P. M.; van Gunsteren, W. F.; DiNola, A.; Haak, J. R. *J. Chem. Phys.* **1984**, *81*, 3684–3690.

- (45) Frenkel, D.; Smith, B. *Understanding Molecular Simulation*; Academic Press: San Diego, 2002.
- (46) Shell, M. S.; Panagiotopoulos, A.; Pohorille, A. Methods Based on Probability Distributions and Histograms. In *Free Energy Calculations*; Chipot, C., Pohorille, A., Eds.; Springer: New York, 2007; pp 77–116.
- (47) Beerdsen, E.; Dubbeldam, D.; Smit, B. *J. Phys. Chem. B* **2006**, *110*, 22754–22772.
- (48) Krishna, R. *J. Phys. Chem. C* **2009**, *113*, 19756–19781.
- (49) Schüring, A.; Gulín-González, J.; Vasenkov, S.; Fritzsche, S. *Microporous Mesoporous Mater.* **2009**, *125*, 107–111.
- (50) Schüring, A. *J. Phys. Chem. C* **2007**, *111*, 11285–11290.
- (51) Hibbe, F.; Chmelik, C.; Heinke, L.; Pramanik, S.; Li, J.; Ruthven, D. M.; Tzoulaki, D.; Kärger, J. *J. Am. Chem. Soc.* **2011**, *133*, 2804–2807.
- (52) Heinke, L.; Kärger, J. *Phys. Rev. Lett.* **2011**, *106*, 074501.
- (53) Choi, M.; Na, K.; Kim, J.; Sakamoto, Y.; Terasaki, O.; Ryoo, R. *Nature* **2009**, *461*, 246–249.
- (54) Perez-Ramirez, J.; Christensen, C. H.; Egeblad, K.; Christensen, C. H.; Groen, J. C. *Chem. Soc. Rev.* **2008**, *37*, 2530–2542.
- (55) Groen, J. C.; Zhu, W.; Brouwer, S.; Huynink, S. J.; Kapteijn, F.; Moulijn, J. A.; Pérez-Ramírez, J. *J. Am. Chem. Soc.* **2007**, *129*, 355–360.
- (56) Valiullin, R.; Kärger, J. *Chem. Ing. Tech.* **2011**, *83*, 166–176.